Editors' Suggestion | Featured in Physics

Topology of Orientational Defects in Confined Smectic Liquid Crystals

Paul A. Monderkamp,[1] René Wittmann,[1,*] Louis B. G. Cortes,[2] Dirk G. A. L. Aarts,[3] Frank Smallenburg,[4] and Hartmut Löwen[1]

[1]*Institut für Theoretische Physik II: Weiche Materie, Heinrich-Heine-Universität Düsseldorf, Universitätsstraße 1, 40225 Düsseldorf, Germany*

[2]*School of Applied and Engineering Physics, Cornell University, Ithaca, New York 14853, USA*

[3]*Department of Chemistry, Physical and Theoretical Chemistry Laboratory, University of Oxford, South Parks Road, Oxford OX1 3QZ, United Kingdom*

[4]*Laboratoire de Physique des Solides, CNRS, Université Paris-Saclay, 91405 Orsay, France*

(Received 8 March 2021; revised 28 June 2021; accepted 22 September 2021; published 3 November 2021)

We propose a general formalism to characterize orientational frustration of smectic liquid crystals in confinement by interpreting the emerging networks of grain boundaries as objects with a topological charge. In a formal idealization, this charge is distributed in pointlike units of quarter-integer magnitude, which we identify with tetratic disclinations located at the end points and nodes. This coexisting nematic and tetratic order is analyzed with the help of extensive Monte Carlo simulations for a broad range of two-dimensional confining geometries as well as colloidal experiments, showing how the observed defect networks can be universally reconstructed from simple building blocks. We further find that the curvature of the confining wall determines the anchoring behavior of grain boundaries, such that the number of nodes in the emerging networks and the location of their end points can be tuned by changing the number and smoothness of corners, respectively.

DOI: 10.1103/PhysRevLett.127.198001

Topological defects are ubiquitous in ordered states of matter [1–5] and thus also emerge as a characteristic feature of liquid crystals [6–11], which exhibit various degrees of positional and orientational ordering [6,12–17]. Frustrated orientational order in nematic liquid crystals typically manifests itself in the form of singular points or lines. Defects of this type may spontaneously form and annihilate in bulk due to fluctuations [18], external influences such as electromagnetic fields [19–23], changes in temperature [24,25], or active motion [26–28]. In these processes, the defect strength, quantified by a half-integer topological charge Q, is subject to a universal conservation law [29,30]. The formation of topological defects can further be triggered in a controlled manner through confining the particles [31–47] or inserting an obstacle [48–55]. In this case, the precise type, number, and location of defects depend on the particular geometry [56–58] and particle properties [43,59–62], due to a delicate balance between elastic distortions and surface anchoring.

The characteristic positional order of smectic liquid crystals breaks the symmetry of the homogeneous nematic phase and affects the elastic properties [6,63]. The constraints associated with the layer structure [64,65] stabilize distortions of the bulk smectic lattice [66,67] which do not exist in nematic liquid crystals [6]. These include purely positional defects called edge dislocations [68–71] but also more complex objects like focal conic domains [72–75]. In many cases, orientational frustration in smectic phases can be well described in terms of topological defects in the nematic order that is inherent to the symmetry of the smectic phase. However, in the paradigmatic case of confined two-dimensional lyotropic systems, the formation of grain boundaries largely dominates over strong elastic deformations [76–78]. At these grain boundaries, the nematic order present in the bulk smectic phase breaks down, hindering a classification of the emerging orientational patterns in terms of nematic topology alone.

In this Letter, we demonstrate that extremely confined smectic systems can be effectively described in terms of topological defects in the tetratic order due to the strong preference of smectic layers to tilt at a grain boundary by approximately 90°. The tetratic topology is thus not only important in systems with tetratic bulk symmetry [79–82] but also a vital ingredient to a comprehensive picture of frustrated smectics. In detail, we identify quarter-integer tetratic disclinations, which materialize in pairs at the extremities of grain boundaries, as the elementary topological unit of smectic liquid crystals. In turn, the notion of a nematic disclination expands to a spatially extended defect structure whose half-integer charge follows from the sum of its tetratic components, thereby acting as a spatial charge distribution, as exemplified in Fig. 1. To unveil the full implications of coexisting nematic and tetratic order, we use particle-resolved computer simulations and colloidal experiments on hard rods to create different defect structures in a large range of two-dimensional geometries.

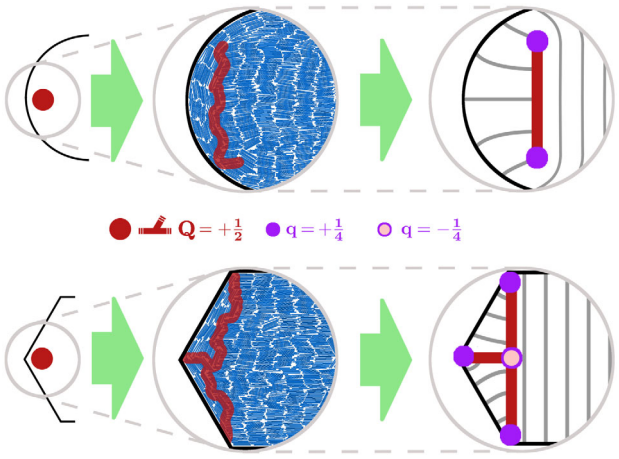

FIG. 1. Topological characterization of grain boundaries in confined smectic liquid crystals. Left: coarse-grained topological structure with an idealized nematic disclination of half-integer charge Q induced by the presumed planar alignment with the nearby wall. Middle: particle-resolved simulation snapshots of hard rods with highlighted grain boundaries in the form of a line close to a circular wall (top row) and a network induced by corners (bottom row). Right: continuum model with quarter-integer tetratic point charges q at the end points and nodes, which can be interpreted as the distribution of the spatially extended charge Q.

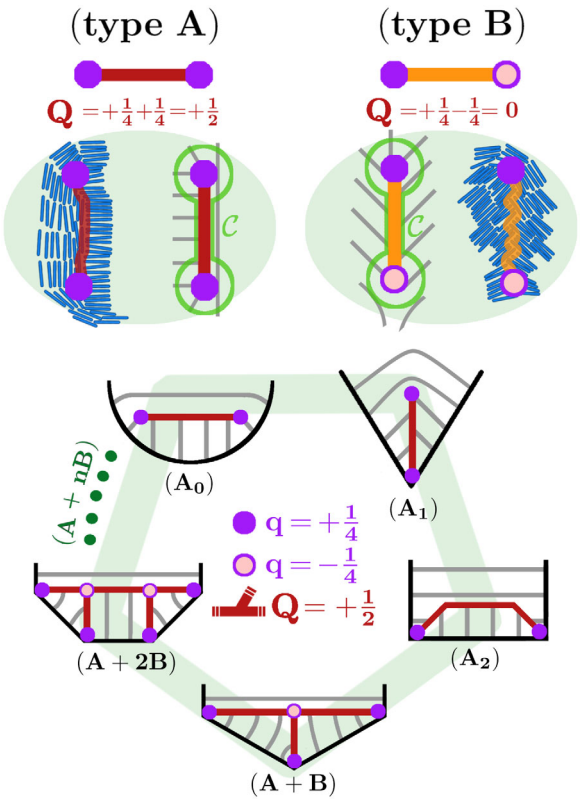

FIG. 2. Survey of grain boundaries with different connectivities in smectic liquid crystals at a convex confining wall. Top: composition of the two fundamental building blocks with total nematic charge $Q = 1/2$ (type A, red line) and $Q = 0$ (type B, orange line), determined by the tetratic quarter charges q (dots) at the end points. The illustration of bulk orientational ordering depicts a typical arrangement of the surrounding rods and a schematic continuum picture with idealized straight grain boundaries separating regions of perpendicular smectic layers (grey lines). The closed contour $\mathcal{C}$ (green line) highlights the contribution of the tetratic end points to $Q = \sum q$. Bottom: relation between the geometry-dependent manifestations of $Q = +1/2$ grain-boundary networks (red) in smectics confined to polygons. The simplest structure (A_m) only contains one type-A defect with $m \in \{0, 1, 2\}$ of its end points attached to a corner of the confining wall. In general, complex networks $(A + nB)$ can form, which amounts to adding n building blocks of type B. Approaching the limit $n \to \infty$, the network detaches from the increasingly smooth corners, gradually reverting to (A_0), as the tetratic defects in the type-B branches annihilate [83].

Defining the grain boundaries connecting different types of tetratic disclinations as fundamental building blocks, we provide the basic toolbox to characterize the more complex smectic defect networks emerging in the presence of multiple corners, as illustrated in Fig. 2. Thereby, our approach visualizes the topological charge conservation $\sum q = \sum Q = 1$ for both individual tetratic point defects q and defect networks with nematic charge Q, whose typical connectivity depends on the curvature landscape of the confining wall.

To create the smectic structures for each confinement, we perform canonical Monte Carlo (MC) simulations on $N = 1000$ hard discorectangles [84] of aspect ratio $p = 15$ within two-dimensional cavities, bounded by WCA-like soft walls [85,86]; see Supplemental Material [83]. We randomly initialize the system at a low area fraction $\eta_0 \ll 1$. The system is quickly compressed at a rate of $\Delta\eta_1 = 4.15 \times 10^{-7}$ per MC cycle to an area fraction $\eta_1 \approx 0.29$, where the isotropic-nematic transition is expected [87]. We subsequently compress the system at a lower rate $\Delta\eta_2 = 4.625 \times 10^{-8}$ per MC cycle until the system reaches the target area fraction of $\eta_2 = 0.75$ and exhibits smectic order. This protocol ensures that the system is close to equilibrium at all times. After equilibration, we use cluster analysis to identify domains with different orientational order and generate statistics. For each state, we determine local nematic $S(\mathbf{r})$ and tetratic $T(\mathbf{r})$ order parameter fields to identify the composition of topological defects [83].

On the experimental side, we analyze smectic structures emerging at the bottom of tailored cavities at sedimentation-diffusion equilibrium of colloidal silica rods [77]. The synthetic rods [88] have a small polydispersity in length and diameter. They are dispersed into a 1 mM NaCl aqueous solution [78], which leads to a short-ranged repulsion and effective hard-rod-like interactions. The degenerate planar anchoring at the bottom wall allows us to capture images of quasi-two-dimensional smectic states in the horizontal plane. Using bright-field

microscopy with an objective of high numerical aperture, we can discriminate most rods and thus determine the local order.

Our numerical observations are summarized in Fig. 3. The common feature of all structures is a large, defect-free central domain, characteristic for the bridge state [76–78]. The detailed appearance of the topological defects, however, sensitively depends on the confining geometry. To verify that the overall topology is universal, we decorate [83] all representative snapshots with a defect structure assembled from the building blocks in Fig. 2. By doing so, we recognize in each system in Fig. 3 two separate grain-boundary networks representing a $Q = +1/2$ charge each, while the remaining defects do not carry any nematic charge Q as a whole. The intriguing dependence of the emerging defect networks on the geometric properties of the confining wall can be perceived according to the schematic cycle in Fig. 2, as laid out in the following three paragraphs.

The most common defects are linear grain boundaries of the general type A, which we further discriminate by the location of the two positively charged tetratic end points, cf. Fig. 2. The circular cavity in Fig. 3 typically features two opposing bulk defects of subtype A_0, i.e., both end points possessing isolated tetratic signals are detached from the wall. Therefore, the orientation of rods around the perimeter changes continuously and all particles within the system belong to a single domain. Upon switching from the uniformly curved circular confinement to different polygons, the grain boundaries usually extend towards the corners, such that the tetratic defects anchor at the wall. The invariance of our topological picture can be illustrated by considering confinements with smooth corners [83]. The example of a rounded equilateral triangle in Fig. 3 indicates

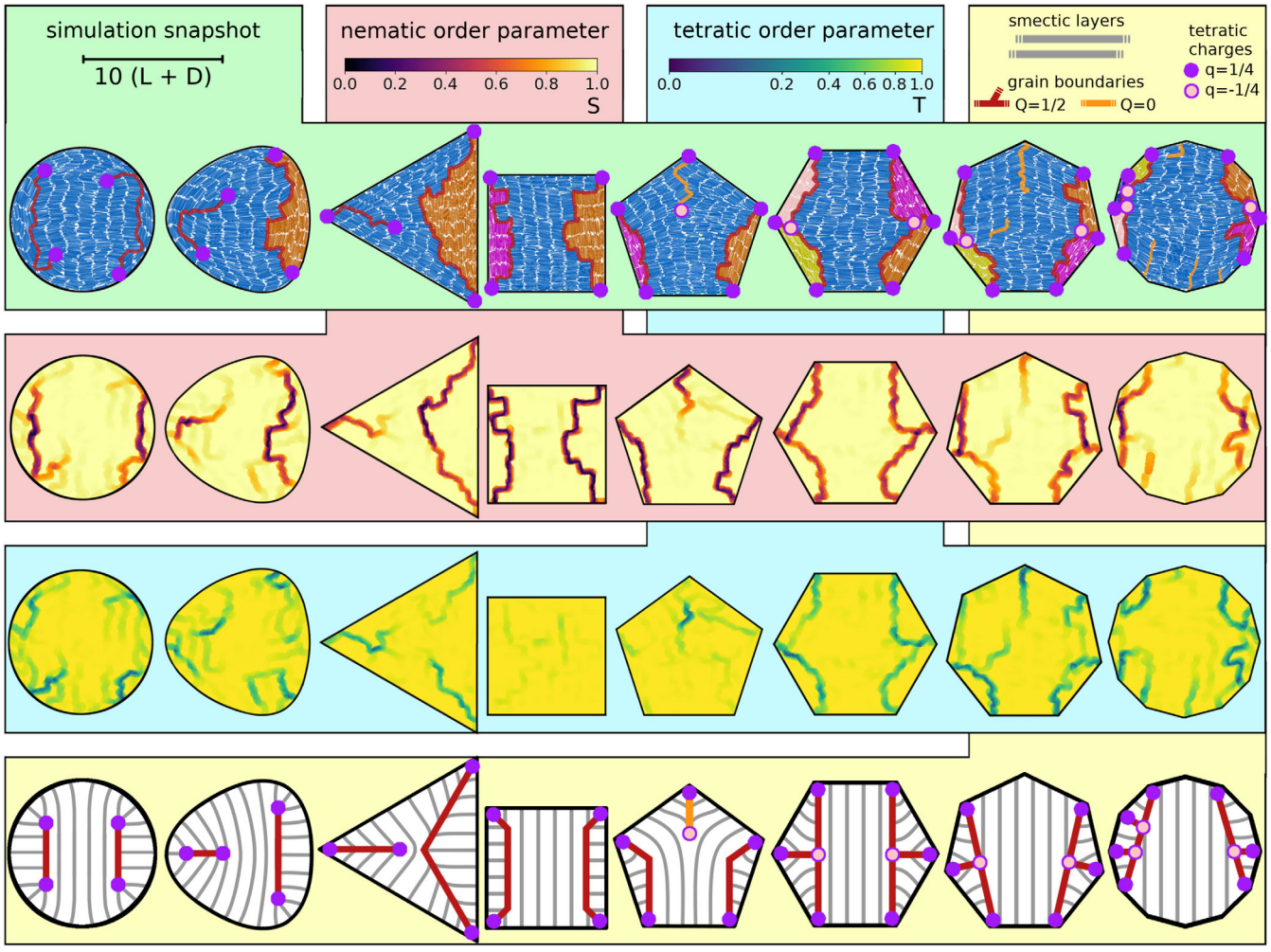

FIG. 3. Topological defect structure of representative simulations for hard rods with aspect ratio $p = 15$ in different convex confining geometries. Top row: particle snapshots with superimposed networks of grain boundaries and isolated tetratic point defects, compare Fig. 2. The color of the rods highlights individual domains according to cluster analysis. Second row: nematic order parameter field $S(\mathbf{r})$. Third row: tetratic order parameter field $T(\mathbf{r})$. Point defects at the confining wall are not visible. Bottom row: idealized continuum interpretation of the depicted snapshots, as detailed in the Supplemental Material [83].

that one grain boundary turns into a true domain boundary, i.e., a type-A_2 defect, as both its end points move towards two of the three corners. The second grain boundary gradually turns into a type-A_1 defect, as one end point attaches with the remaining corner and the other end extends into the center of the large domain. This structure is most pronounced in the limit of sharp corners. We further observe that a grain boundary of type A_1 gradually contracts to a $Q = +1/2$ point defect upon decreasing the opening angle [83]. Turning to a square cavity in Fig. 3, the additional corner can accommodate the loose end point of the type-A_1 defect, resulting in the eponymous bridge structure [76,77] with two parallel type-A_2 domain boundaries, as in circular confinement, but with perfect tetratic bulk order.

Following in Fig. 3 a sequence of geometries represented by regular polygons, the increasing number of $q = +1/4$ charges at each corner is compensated accordingly by negative bulk charges. We thus introduce an additional type-B building block representing a pair of tetratic $q = \pm 1/4$ charges. This overall charge-neutral object with $Q = 0$ either occurs on its own (at edge dislocations in the bulk or attached to a single corner) or attaches with its negative end to other building blocks, forming a large network of grain boundaries, cf. Fig. 2. In particular, the pentagon can accommodate an individual type-B defect in addition to the two type-A_2 domain boundaries also found in square confinement (notice the difference with the free-standing type-A_1 defect with $Q = 1/2$ in the triangle). The hexagon typically features two parallel type-$(A + B)$ networks, each separating two small domains from the central bridging layers and resembling a type-A defect, like in the square, with an attached type-B defect emerging from the additional corner in the middle.

The addition of further corners allows for the formation of complex type-$(A + nB)$ networks, which contain n nodes with $q = -1/4$ and $n + 2$ branches ending on a $q = +1/4$ charge. The typical defect structure, however, gradually reverts to that in circular confinement, closing the cycle in Fig. 2. The defect networks in Fig. 3 thus detach from the confining wall, as adjacent pairs of opposite tetratic charges annihilate. Grain boundaries between pairs of defects close to annihilation typically induce only a small tilt between smectic layers, such that their nematic signal weakens and qualitatively resembles the tetratic signal (contrast, e.g., the free-standing type-B defects in the pentagon and heptagon). In general, the degree of the annihilation increases with increasing opening angle at the corners [83].

To demonstrate the experimental relevance of our classification scheme, we analyze in Fig. 4 microscopy images of colloidal rods for their orientational order, here focusing on a hexagonal domain. The experimental defect networks are typically less complex than those in the pure hard-rod simulations [83], due to the higher elasticity of the smectic layers. Nonetheless, the defect networks found consist of the same fundamental building blocks, confirming the broad applicability of our approach. Additionally, our simulation results match the previously reported experiments in square [77] and circular [78] confinement, and hence the same analysis is directly suitable to those experiments as well.

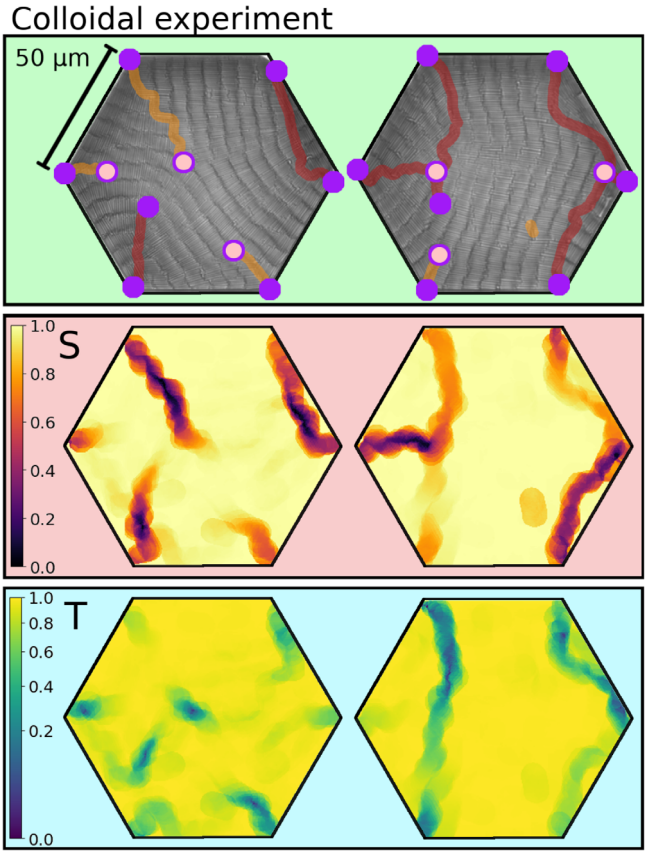

FIG. 4. Two selected sets of experimental reference data in hexagonal confinement, presented as in Fig. 3. Shown are bare bright-field microscopy images with $N = 1400 \pm 150$ colloidal rods of effective hard-rod aspect ratio $p_{\mathrm{eff}} = 10.6$ in the field of view and the extracted order parameters.

Beyond the chosen methodology, our topological toolbox can be readily employed to illustrate the coexisting nematic and tetratic orientational order of frustrated smectics in free-energy based theoretical studies [15,78,89–91], granular experiments [80–82] or molecular systems [92–94]. Regarding nonconvex confinements [78] or two-dimensional manifolds [65,95], our set of building blocks can be supplemented by a line connecting two negative tetratic charges. A generalized approach can shed more light on intersecting surfaces of grain boundaries in three-dimensions. One central implication of our analysis is that the motion of grain boundaries can be tracked through tetratic point defects, providing additional insights into the dynamics of smectics [96–99] and their nucleation [100–102], which is particularly interesting for biologically inspired nonequilibrium systems

like self-propelled rods [103–106] or growing bacterial colonies [107–109] as candidates for active smectics.

Finally, we expect that the classification of the fine structure of defects on the length scale of individual particles put forward in this work will be helpful to analyze quenched or undercooled systems, in particular those where the symmetry of an ordered phase is broken by grain boundaries that may still impose a preferred alignment between adjacent domains. One possible example would be fine-grained polycrystals, which are challenging to distinguish from amorphous solids on the single-particle level [110]. More generally, those methods could lead to a better understanding of defects in complex solids (such as protein [111] or aerosol [112] crystals) relevant for photonics [113], phononics [114] and metamaterials [115].

The authors would like to thank Daniel de las Heras, Axel Voigt, Raphael Wittkowski, and Michael te Vrugt for helpful discussions. This work was supported by the German Research Foundation (DFG) within project LO 418/20-2.

P. M. and R. W. contributed equally to this work.

*rene.wittmann@hhu.de

[1] P. M. Chaikin and T. C. Lubensky, *Topological Defects* (Cambridge University Press, Cambridge, England, 1995), pp. 495–589.
[2] N. D. Mermin, Rev. Mod. Phys. **51**, 591 (1979).
[3] T. W. B. Kibble, J. Phys. A **9**, 1387 (1976).
[4] A. Moor, A. F. Volkov, and K. B. Efetov, Phys. Rev. B **90**, 224512 (2014).
[5] Y. Liu, Z. Wang, T. Sato, M. Hohenadler, C. Wang, W. Guo, and F. F. Assaad, Nat. Commun. **10**, 2658 (2019).
[6] P.-G. de Gennes and J. Prost, *The Physics Of Liquid Crystals* (Clarendon Press, Oxford, 1993).
[7] M. Kleman and O. D. Lavrentovich, *Soft Matter Physics—An Introduction* (Springer-Verlag, Berlin, 2003).
[8] G. P. Alexander, B. G. -g. Chen, E. A. Matsumoto, and R. D. Kamien, Rev. Mod. Phys. **84**, 497 (2012).
[9] K. Sentker, A. W. Zantop, M. Lippmann, T. Hofmann, O. H. Seeck, A. V. Kityk, A. Yildirim, A. Schönhals, M. G. Mazza, and P. Huber, Phys. Rev. Lett. **120**, 067801 (2018).
[10] S. Čopar, N. A. Clark, M. Ravnik, and S. Žumer, Soft Matter **9**, 8203 (2013).
[11] L. Radzihovsky, Phys. Rev. Lett. **125**, 267601 (2020).
[12] R. Teerakapibal, C. Huang, A. Gujral, M. D. Ediger, and L. Yu, Phys. Rev. Lett. **120**, 055502 (2018).
[13] P. Bolhuis and D. Frenkel, J. Chem. Phys. **106**, 666 (1997).
[14] L. Mederos, E. Velasco, and Y. Martínez-Ratón, J. Phys. Condens. Matter **26**, 463101 (2014).
[15] R. Wittmann, C. E. Sitta, F. Smallenburg, and H. Löwen, J. Chem. Phys. **147**, 134908 (2017).
[16] S. Dussi, N. Tasios, T. Drwenski, R. van Roij, and M. Dijkstra, Phys. Rev. Lett. **120**, 177801 (2018).
[17] V. F. D. Peters, M. Vis, A. G. García, H. H. Wensink, and R. Tuinier, Phys. Rev. Lett. **125**, 127803 (2020).
[18] G. P. Crawford and S. Zumer, *Liquid Crystals in Complex Geometries: Formed by Polymer and Porous Networks* (CRC Press, London, 1996), https://doi.org/10.1201/9781482272796.
[19] Y. Reznikov, O. Ostroverkhova, K. D. Singer, J.-H. Kim, S. Kumar, O. Lavrentovich, B. Wang, and J. L. West, Phys. Rev. Lett. **84**, 1930 (2000).
[20] Y. Gu and N. L. Abbott, Phys. Rev. Lett. **85**, 4719 (2000).
[21] H. Stark, Phys. Rev. E **66**, 032701 (2002).
[22] P. E. Cladis, W. van Saarloos, P. L. Finn, and A. R. Kortan, Phys. Rev. Lett. **58**, 222 (1987).
[23] D. R. Link, J. E. Maclennan, and N. A. Clark, Phys. Rev. Lett. **77**, 2237 (1996).
[24] T. Ohzono and J.-i. Fukuda, Soft Matter **8**, 11552 (2012).
[25] C. D. Muzny and N. A. Clark, Phys. Rev. Lett. **68**, 804 (1992).
[26] X.-Q. Shi and Y.-Q. Ma, Nat. Commun. **4**, 3013 (2013).
[27] V. Narayan, S. Ramaswamy, and N. Menon, Science **317**, 105 (2007).
[28] A. Chardac, L. A. Hoffmann, Y. Poupart, L. Giomi, and D. Bartolo, arXiv:2103.03861 [Phys. Rev. X (to be published)].
[29] W. Fulton, *Algebraic Topology—A First Course* (Springer-Verlag, Berlin, 1995).
[30] B. Senyuk, Q. Liu, S. He, R. D. Kamien, R. B. Kusner, T. C. Lubensky, and I. I. Smalyukh, Nature (London) **493**, 200 (2013).
[31] O. D. Lavrentovich and E. M. Terentjev, Zh. Eksp. Teor. Fiz. **91**, 2084 (1986).
[32] O. D. Lavrentovich, Liq. Cryst. **24**, 117 (1998).
[33] Y.-K. Kim, S. V. Shiyanovskii, and O. D. Lavrentovich, J. Condens. Matter Phys. **25**, 404202 (2013).
[34] O. J. Dammone, I. Zacharoudiou, R. P. A. Dullens, J. M. Yeomans, M. P. Lettinga, and D. G. A. L. Aarts, Phys. Rev. Lett. **109**, 108303 (2012).
[35] O. V. Manyuhina, K. B. Lawlor, M. C. Marchetti, and M. J. Bowick, Soft Matter **11**, 6099 (2015).
[36] J. Dzubiella, M. Schmidt, and H. Löwen, Phys. Rev. E **62**, 5081 (2000).
[37] Y. Trukhina and T. Schilling, Phys. Rev. E **77**, 011701 (2008).
[38] S. Varga, Y. Martínez-Ratón, and E. Velasco, J. Phys. Condens. Matter **26**, 075104 (2014).
[39] P. E. Brumby, H. H. Wensink, A. J. Haslam, and G. Jackson, Langmuir **33**, 11754 (2017).
[40] A. H. Lewis, I. Garlea, J. Alvarado, O. J. Dammone, P. D. Howell, A. Majumdar, B. M. Mulder, M. Lettinga, G. H. Koenderink, and D. G. A. L. Aarts, Soft Matter **10**, 7865 (2014).
[41] S. Kralj and A. Majumdar, Proc. R. Soc. A **470**, 20140276 (2014).
[42] A. Majumdar and A. Lewis, Liq. Cryst. **43**, 2332 (2016).
[43] I. C. Gârlea, P. Mulder, J. Alvarado, O. J. Dammone, D. G. A. L. Aarts, M. P. Lettinga, G. H. Koenderink, and B. M. Mulder, Nat. Commun. **7**, 12112 (2016).
[44] M. V. Kurik and O. D. Lavrentovich, Sov. Phys. Usp. **31**, 196 (1988).
[45] X. Yao and J. Z. Y. Chen, Phys. Rev. E **101**, 062706 (2020).
[46] E. Basurto, P. Gurin, S. Varga, and G. Odriozola, Phys. Rev. Research **2**, 013356 (2020).
[47] K. H. Kil, A. Yethiraj, and J. S. Kim, Phys. Rev. E **101**, 032705 (2020).

[48] P. Poulin, V. Cabuil, and D. A. Weitz, Phys. Rev. Lett. **79**, 4862 (1997).
[49] R. W. Ruhwandl and E. M. Terentjev, Phys. Rev. E **56**, 5561 (1997).
[50] D. Andrienko, G. Germano, and M. P. Allen, Phys. Rev. E **63**, 041701 (2001).
[51] S. Čopar, T. Porenta, V. S. R. Jampani, I. Muševič, and S. Žumer, Soft Matter **8**, 8595 (2012).
[52] J. M. Ilnytskyi, A. Trokhymchuk, and M. Schoen, J. Chem. Phys. **141**, 114903 (2014).
[53] S. Püschel-Schlotthauer, V. Meiwes Turrin, C. K. Hall, M. G. Mazza, and M. Schoen, Langmuir **33**, 2222 (2017).
[54] B. Senyuk, Q. Liu, Y. Yuan, and I. I. Smalyukh, Phys. Rev. E **93**, 062704 (2016).
[55] K. Chen, O. J. Gebhardt, R. Devendra, G. Drazer, R. D. Kamien, D. H. Reich, and R. L. Leheny, Soft Matter **14**, 83 (2018).
[56] T. Araki, F. Serra, and H. Tanaka, Soft Matter **9**, 8107 (2013).
[57] M. G. Campbell, M. Tasinkevych, and I. I. Smalyukh, Phys. Rev. Lett. **112**, 197801 (2014).
[58] I. C. Gârlea, O. Dammone, J. Alvarado, V. Notenboom, Y. Jia, G. H. Koenderink, D. G. A. L. Aarts, M. P. Lettinga, and B. M. Mulder, Sci. Rep. **9**, 20391 (2019).
[59] G. van Anders, D. Klotsa, N. K. Ahmed, M. Engel, and S. C. Glotzer, Proc. Natl. Acad. Sci. U.S.A. **111**, E4812 (2014).
[60] J. Alvarado, B. M. Mulder, and G. H. Koenderink, Soft Matter **10**, 2354 (2014).
[61] M. Chiappini, T. Drwenski, R. van Roij, and M. Dijkstra, Phys. Rev. Lett. **123**, 068001 (2019).
[62] D. Revignas and A. Ferrarini, Phys. Rev. Lett. **125**, 267802 (2020).
[63] J. P. F. Lagerwall and F. Giesselmann, ChemPhysChem **7**, 20 (2006).
[64] V. Poénaru, Commun. Math. Phys. **80**, 127 (1981).
[65] R. A. Mosna, D. A. Beller, and R. D. Kamien, Phys. Rev. E **86**, 011707 (2012).
[66] B. G. -g. Chen, G. P. Alexander, and R. D. Kamien, Proc. Natl. Acad. Sci. U.S.A. **106**, 15577 (2009).
[67] T. Machon, H. Aharoni, Y. Hu, and R. D. Kamien, Commun. Math. Phys. **372**, 525 (2019).
[68] R. B. Meyer, B. Stebler, and S. T. Lagerwall, Phys. Rev. Lett. **41**, 1393 (1978).
[69] P. Chen and C.-Y. D. Lu, J. Phys. Soc. Jpn. **80**, 094802 (2011).
[70] C. Zhang, A. M. Grubb, A. J. Seed, P. Sampson, A. Jákli, and O. D. Lavrentovich, Phys. Rev. Lett. **115**, 087801 (2015).
[71] R. D. Kamien and R. A. Mosna, New J. Phys. **18**, 053012 (2016).
[72] M. Kléman and O. Lavrentovich, Eur. Phys. J. E **2**, 47 (2000).
[73] J. P. Bramble, S. D. Evans, J. R. Henderson, T. J. Atherton, and N. J. Smith, Liq. Cryst. **34**, 1137 (2007).
[74] Y. H. Kim, D. K. Yoon, M.-C. Choi, H. S. Jeong, M. W. Kim, O. D. Lavrentovich, and H.-T. Jung, Langmuir **25**, 1685 (2009).
[75] D. B. Liarte, M. Bierbaum, R. A. Mosna, R. D. Kamien, and J. P. Sethna, Phys. Rev. Lett. **116**, 147802 (2016).
[76] T. Geigenfeind, S. Rosenzweig, M. Schmidt, and D. de las Heras, J. Chem. Phys. **142**, 174701 (2015).
[77] L. B. G. Cortes, Y. Gao, R. P. A. Dullens, and D. G. A. L. Aarts, J. Phys. Condens. Matter **29**, 064003 (2017).
[78] R. Wittmann, L. B. G. Cortes, H. Löwen, and D. G. A. L. Aarts, Nat. Commun. **12**, 623 (2021).
[79] Y. Li, H. Miao, H. Ma, and J. Z. Y. Chen, Soft Matter **9**, 11461 (2013).
[80] V. Narayan, N. Menon, and S. Ramaswamy, J. Stat. Mech. (2006) P01005.
[81] M. González-Pinto, F. Borondo, Y. Martínez-Ratón, and E. Velasco, Soft Matter **13**, 2571 (2017).
[82] A. D.-D. Armas, M. Maza-Cuello, Y. Martínez-Ratón, and E. Velasco, Phys. Rev. Research **2**, 033436 (2020).
[83] See Supplemental Material at http://link.aps.org/supplemental/10.1103/PhysRevLett.127.198001 for a detailed description of the physical model, simulation procedure and analysis of the observed topological structures. We also discuss some additional simulation results for different isosceles triangles, triangles with rounded corners and explore the dependence on system size, aspect ratio and density.
[84] C. Vega and S. Lago, Comput. Chem. **18**, 55 (1994).
[85] H. C. Andersen, D. Chandler, and J. D. Weeks, J. Chem. Phys. **56**, 3812 (1972).
[86] N. Metropolis, A. W. Rosenbluth, M. N. Rosenbluth, A. H. Teller, and E. Teller, J. Chem. Phys. **21**, 1087 (1953).
[87] M. A. Bates and D. Frenkel, J. Chem. Phys. **112**, 10034 (2000).
[88] A. Kuijk, D. V. Byelov, A. V. Petukhov, A. van Blaaderen, and A. Imhof, Faraday Discuss. **159**, 181 (2012).
[89] R. Wittmann, M. Marechal, and K. Mecke, J. Phys. Condens. Matter **28**, 244003 (2016).
[90] M. Y. Pevnyi, J. V. Selinger, and T. J. Sluckin, Phys. Rev. E **90**, 032507 (2014).
[91] J. Xia, S. MacLachlan, T. J. Atherton, and P. E. Farrell, Phys. Rev. Lett. **126**, 177801 (2021).
[92] J. Jeong and M. W. Kim, Phys. Rev. Lett. **108**, 207802 (2012).
[93] J.-P. Michel, E. Lacaze, M. Goldmann, M. Gailhanou, M. de Boissieu, and M. Alba, Phys. Rev. Lett. **96**, 027803 (2006).
[94] D. Coursault, B. Zappone, A. Coati, A. Boulaoued, L. Pelliser, D. Limagne, N. Boudet, B. H. Ibrahim, A. de Martino, M. Alba *et al.*, Soft Matter **12**, 678 (2016).
[95] E. Allahyarov, A. Voigt, and H. Löwen, Soft Matter **13**, 8120 (2017).
[96] J. K. G. Dhont, *An Introduction to Dynamics of Colloids* (Elsevier, New York, 1996), vol. 2.
[97] E. Grelet, M. P. Lettinga, M. Bier, R. van Roij, and P. van der Schoot, J. Phys. Condens. Matter **20**, 494213 (2008).
[98] R. Kurita, S. Mitsui, and H. Tanaka, Phys. Rev. Lett. **119**, 108003 (2017).
[99] M. Chiappini, E. Grelet, and M. Dijkstra, Phys. Rev. Lett. **124**, 087801 (2020).
[100] T. Schilling and D. Frenkel, Phys. Rev. Lett. **92**, 085505 (2004).
[101] R. Ni, S. Belli, R. van Roij, and M. Dijkstra, Phys. Rev. Lett. **105**, 088302 (2010).

[102] A. Cuetos, E. Sanz, and M. Dijkstra, Faraday Discuss. **144**, 253 (2010).
[103] M. Bär, R. Großmann, S. Heidenreich, and F. Peruani, Annu. Rev. Condens. Matter Phys. **11**, 441 (2020).
[104] N. Kumar, R. K. Gupta, H. Soni, S. Ramaswamy, and A. K. Sood, Phys. Rev. E **99**, 032605 (2019).
[105] A. Maitra, P. Srivastava, M. C. Marchetti, S. Ramaswamy, and M. Lenz, Phys. Rev. Lett. **124**, 028002 (2020).
[106] M. C. Bott, F. Winterhalter, M. Marechal, A. Sharma, J. M. Brader, and R. Wittmann, Phys. Rev. E **98**, 012601 (2018).
[107] D. van Holthe tot Echten, G. Nordemann, M. Wehrens, S. Tans, and T. Idema, arXiv:2003.10509.
[108] Z. You, D. J. G. Pearce, and L. Giomi, Sci. Adv. **7**, abc8685 (2021).
[109] K. Copenhagen, R. Alert, N. S. Wingreen, and J. W. Shaevitz, Nat. Phys. **17**, 211 (2021).
[110] H. Zhang and Y. Han, Phys. Rev. X **8**, 041023 (2018).
[111] D. S. Tsekova, D. R. Williams, and J. Y. Heng, Chem. Eng. Sci. **77**, 201 (2012).
[112] U. Dusek, G. Frank, L. Hildebrandt, J. Curtius, J. Schneider, S. Walter, D. Chand, F. Drewnick, S. Hings, D. Jung *et al.*, Science **312**, 1375 (2006).
[113] L. Lu, J. D. Joannopoulos, and M. Soljačić, Nat. Photonics **8**, 821 (2014).
[114] G. Yi and B. D. Youn, Struct. Multidiscip. Optim. **54**, 1315 (2016).
[115] Y.-F. Wang, Y.-Z. Wang, B. Wu, W. Chen, and Y.-S. Wang, Appl. Mech. Rev. **72**, 040801 (2020).